A&A 591, A53 (2016)
DOI: 10.1051/0004-6361/201628106


Astronomy & Astrophysics

# High-resolution abundance analysis of red giants in the metal-poor bulge globular cluster HP 1⋆

B. Barbuy[1], E. Cantelli[1], A. Vemado[1], H. Ernandes[1], S. Ortolani[2,3], I. Saviane[4], E. Bica[5], D. Minniti[6,7], B. Dias[4], Y. Momany[3], V. Hill[8], M. Zoccali[6,9], and C. Siqueira-Mello[1]

[1] Universidade de São Paulo, IAG, Rua do Matão 1226, Cidade Universitária, 05508-900 São Paulo, Brazil
e-mail: barbuy@astro.iag.usp.br
[2] Dipartimento di Fisica e Astronomia, Università di Padova, 35122 Padova, Italy
[3] INAF–Osservatorio Astronomico di Padova, Vicolo dell'Osservatorio 5, 35122 Padova, Italy
[4] European Southern Observatory, Alonso de Cordova 3107, Santiago, Chile
[5] Universidade Federal do Rio Grande do Sul, Departamento de Astronomia, CP 15051, 91501-970 Porto Alegre, Brazil
[6] Millenium Institute of Astrophysics, Av. Vicuña Mackenna 4860, Macul, Santiago, Chile
[7] Departamento de Ciencias Fisicas, Universidad Andres Bello, Republica 220, Santiago, Chile
[8] Laboratoire Lagrange (UMR 7293), Université de Nice Sophia Antipolis, CNRS, Observatoire de la Côte d'Azur, CS 34229, 06304 Nice Cedex 4, France
[9] Pontificia Universidad Catolica de Chile, Instituto de Astrofisica, Casilla 306, Santiago 22, Chile

Received 11 January 2016 / Accepted 31 March 2016

**ABSTRACT**

*Context.* The globular cluster HP 1 is projected at only 3°.33 from the Galactic center. Together with its distance, this makes it one of the most central globular clusters in the Milky Way. It has a blue horizontal branch (BHB) and a metallicity of [Fe/H] ≈ −1.0. This means that it probably is one of the oldest objects in the Galaxy. Abundance ratios can reveal the nucleosynthesis pattern of the first stars as well as the early chemical enrichment and early formation of stellar populations.
*Aims.* High-resolution spectra obtained for six stars were analyzed to derive the abundances of the light elements C, N, O, Na, and Al, the alpha-elements Mg, Si, Ca, and Ti, and the heavy elements Sr, Y, Zr, Ba, La, and Eu.
*Methods.* High-resolution spectra of six red giants that are confirmed members of the bulge globular cluster HP 1 were obtained with the 8 m VLT UT2-Kueyen telescope with the UVES spectrograph in FLAMES-UVES configuration. The spectroscopic parameter derivation was based on the excitation and ionization equilibrium of Fe I and Fe II.
*Results.* We confirm a mean metallicity of [Fe/H] = −1.06 ± 0.10, by adding the two stars that were previously analyzed in HP 1. The alpha-elements O and Mg are enhanced by about +0.3 ≲ [O,Mg/Fe] ≲ +0.5 dex, Si is moderately enhanced with +0.15 ≲ [Si/Fe] ≲ +0.35 dex, while Ca and Ti show lower values of −0.04 ≲ [Ca,Ti/Fe] ≲ +0.28 dex. The r-element Eu is also enhanced with [Eu/Fe] ≈ +0.4, which together with O and Mg is indicative of early enrichment by type II supernovae. Na and Al are low, but it is unclear if Na-O are anticorrelated. The heavy elements are moderately enhanced, with −0.20 < [La/Fe] < +0.43 dex and 0.0 < [Ba/Fe] < +0.75 dex, which is compatible with r-process formation. The spread in Y, Zr, Ba, and La abundances, on the other hand, appears to be compatible with the spinstar scenario or other additional mechanisms such as the weak r-process.

**Key words.** stars: abundances – Galaxy: bulge – globular clusters: individual: HP 1

## 1. Introduction

The globular cluster HP 1 is located at 3°.33 and 1.8 kpc from the Galactic center. This is in the inner bulge volume, and the cluster lies among the globular clusters that are closest to the Galactic center. A metallicity of [Fe/H] ∼ −1.0 was deduced from its color-magnitude diagram (CMD) by Ortolani et al. (1997, 2011). High-resolution spectroscopy of two stars performed by Barbuy et al. (2006) resulted in [Fe/H] = −1.0 ± 0.2, and low-resolution spectroscopy of eight red giants by Dias et al. (2016) yielded a mean of [Fe/H] = −1.17 ± 0.07. Metallicities like this are at the lower end of the metal-poor stellar population in the metallicity distribution function (MDF) of bulge stars by Zoccali et al. (2008), Hill et al. (2011) and Rojas-Arriagada et al. (2014). A lower metallicity end at [Fe/H] ∼ −1.0 is due to the fast chemical enrichment in the Galactic bulge as modeled for example by Cescutti et al. (2008). There are traces of a very metal-poor population in the bulge, such as those found by García-Perez et al. (2013) and Howes et al. (2014, 2015). These stars are very interesting, but most of them are located in the outer bulge and might more probably be halo stars. The main fact is that the bulk of the bulge stars show a lower end at [Fe/H] ∼ −1.0. A metallicity of [Fe/H] ∼ −1.0 could correspond to the population C or D as defined by Ness et al. (2013) in an MDF of a large sample of bulge stars. For a latitude $b = -5°$, Ness et al. found a mean [Fe/H] = −0.66 for population C stars and identified it with the thick-disk population; their population D has a mean [Fe/H] = −1.16 and was identified by them as a metal-weak thick-disk population. It is not clear whether HP 1 fits into these categories.

The following evidence shows that there may be a stellar population peak at [Fe/H] ∼ −1.0 in the bulge: (a) the metallicity distribution of bulge globular clusters was shown to have two peaks at [Fe/H] ≈ −0.5 and [Fe/H] ≈ −1.0 (Bica et al. 2016),

⋆ Observations collected at the European Southern Observatory, Paranal, Chile (ESO), under programs 93.D-0124A, 65.L-0340A, and 172.B-2002.

where a list of known bulge clusters was selected. This had already been pointed out in Barbuy et al. (2006, 2007, 2009) and Rossi et al. (2015). (b) Another piece of evidence that stars of this metallicity are very old and are characteristic of the old Galactic bulge are the findings by Walker & Terndrup (1991), who showed that RR Lyrae in the bulge show a metallicity peak at [Fe/H] $\approx -1.0$ (see also Lee 1992). Based on the MACHO survey, Kunder & Chaboyer (2008) determined a mean [Fe/H] $= -1.25$, with a broad metallicity distribution. Dékány et al. (2013) used the VISTA Variables in the Via Lactea (VVV) survey and obtained a spheroidal and centrally concentrated distribution, with a slight elongation in its center. Using OGLE-III data, Pietrukowicz et al. (2012) derived [Fe/H] $= -1.02 \pm 0.18$, with a barred distribution toward the central parts of the Galaxy. From OGLE-IV Pietrukowicz et al. (2015) obtained a mean [Fe/H] $= -1.025 \pm 0.25$ and a triaxial ellipsoid shape. The outer bulge studied with $10^3$ VVV RR Lyrae by Gran et al. (2016) shows a centrally concentrated spheroidal distribution. (c) More recently, Schultheis et al. (2015) found a peak of bulge field stars at [Fe/H] $\sim -1.0$ that was enhanced in alpha-elements. (d) Schiavon et al. (in prep.) identified a sample of nitrogen-rich stars that also show metallicities of [Fe/H] $\sim -1.0$.

The triaxial ellipsoid shape as well as a cylindrical rotation as found in the bulge radial velocity assay (BRAVA) by Kunder et al. (2012) are expected from the dynamical evolution of an initially small classical bulge and a bar formed later in the disk (Saha et al. 2012). Therefore either a spheroidal or triaxial shape would be consistent with an initially small classical bulge.

In summary, the moderately metal-poor globular clusters in the inner Galactic bulge might be relics of an early generation of long-lived stars formed in the proto-Galaxy. For this reason we have been pursuing the study of these clusters based on spectroscopy (Barbuy et al. 2006, 2007, 2009, 2014), as well as photometry and color-magnitude diagrams (CMDs) corrected for proper motion, as can be found in Ortolani et al. (2011) and Rossi et al. (2015).

In the present work we carry out a detailed analysis with high spectral resolution of six stars of the globular cluster HP 1. This cluster has a blue horizontal branch (BHB) combined with a metallicity of [Fe/H] $\sim -1.0$, which indicates that it is very old. Ortolani et al. (2011) derived the age by plotting HP 1 in the diagram of Fig. 17 by Dotter et al. (2010). From this, they computed an age difference of about 1 Gyr for HP 1 compared to their sample of halo clusters with ∼12.7 Gyr. This means that HP 1 is about 13.7 Gyr old and appears to be one of the oldest globular clusters in the Galaxy.

The cluster HP 1 is located at J2000 $\alpha = 17^{\rm h}31^{\rm m}05.2^{\rm s}$, $\delta = -29°58'54''$, with Galactic coordinates $l = -2.^{\circ}58$, $b = +2.^{\circ}12$.

The globular cluster HP 1 was discovered at the Observatoire de Haute Provence by Dufay et al. (1954). It was first studied through CMDs by Ortolani et al. (1997) by means of $V, I$ colors. Davidge (2000) studied individual stars in the $J, H, K$, and CO filters and estimated [Fe/H] $= -1.6$ for HP 1. Ortolani et al. (2011) used $J, H$, and $K$ with the multiconjugate adaptive optics demonstrator (MAD) at the VLT, applying a proper motion decontamination procedure, making use of the time difference between the NTT observations from 1994 and the VLT/MAD observations in 2008. This allowed producing decontaminated CMDs and computing the orbit of HP 1 in the Galaxy. The CMD proper motion cleaning greatly optimizes the selection of member stars. Ortolani et al. (2011) showed that HP 1 remains confined within the bulge and/or bar. Minniti (1995) employed medium-resolution infrared spectroscopy and measured indices in six stars of HP 1. They obtained a metallicity of [Fe/H] $= -0.56$ and a radial velocity of 60 km s$^{-1}$. Stephens et al. (2004) used medium-resolution infrared spectra of six stars in HP 1 and derived a metallicity of [Fe/H] $= -1.30$. Two stars of HP 1 were observed at high spectral resolution with UVES and were analyzed spectroscopically (Barbuy et al. 2006), program 65.L-0340 (PI: D. Minniti). To provide the most accurate information on the abundance pattern and kinematics of the metal-poor bulge globular clusters, we analyze a more significant number of stars in HP 1 to better identify the characteristics of the probably oldest stellar population in the Galaxy.

In this work we present a detailed abundance analysis using data from the FLAMES-UVES spectrograph at the VLT with a resolution $R \sim 45\,000$ and a signal-to-noise ratio $S/N > 200$ for all sample stars. The MARCS model atmospheres are employed (Gustafsson et al. 2008).

The observations are described in Sect. 2. The photometric effective temperature and gravity are derived in Sect. 3. Spectroscopic parameters are derived in Sect. 4 and abundance ratios are computed in Sect. 5. A discussion is presented in Sect. 6 and conclusions are drawn in Sect. 7.

## 2. Observations

The sample member stars of HP 1 were selected from data corrected for the proper motion that were reported in Ortolani et al. (2011). Figure 1 shows a $JHK_{\rm s}$-combined image of HP 1 from the Vista Variables in the Via Lactea VVV survey (Saito et al. 2012)[1]. The location of the six sample stars together with the two stars previously analyzed in Barbuy et al. (2006) are shown in Fig. 2, with the observed field in a $z$-color image from the VVV survey.

The spectra of individual stars of HP 1 were obtained at the VLT using the UVES spectrograph (Dekker et al. 2000) in FLAMES-UVES mode. The red arm (5800−6800 Å) has the ESO CCD # 20 chip, an MIT backside illuminated, with a size of 4096 × 2048 pixels, and a pixel size of 15 × 15 $\mu$m. The blue arm (4800−5800 Å) uses the ESO Marlene EEV CCD#44 chip, backside illuminated, with a size of 4102 × 2048 pixels, and a pixel size of 15 × 15 $\mu$m. The UVES standard setup 580 yields a resolution $R \sim 45\,000$ for a slit width of 1 arcsec. The pixel scale is 0.0147 Å/pix, with ∼7.5 pixels per resolution element at 6000 Å. The data were reduced using the UVES pipeline within the ESO/Reflex software (Ballester et al. 2000; Modigliani et al. 2004). The log of the 2014 observations is given in Table 1. The spectra were flat fielded, optimally extracted, and wavelength calibrated with the FLAMES-UVES pipeline. Spectra extracted from different frames were then co-added, taking into account the radial velocities reported in Table 2. The present UVES observations centered on 5800 Å yield a spectral coverage of $4800 < \lambda < 6800$ Å, with a gap at 5708−5825 Å.

We measured the radial velocities of each run using the IRAF FXCOR cross-correlation method, as reported in Table 2. The mean errors reported from the IRAF routine are 1.52 km s$^{-1}$. These values are clearly higher than jitter variations, which are estimated to be around 0.1 km s$^{-1}$ (e.g., Hekker et al. 2008).

The present mean heliocentric radial velocity $v_{\rm r}^{\rm hel} = +40.0 \pm 0.5$ km s$^{-1}$ agrees very well with the value of +45.8 km s$^{-1}$ derived from two stars in Barbuy et al. (2006). These are very low radial velocities, which combined with the low proper motions (Ortolani et al. 2011) support the possibility of a confinement in the bulge.

[1] http://horus.roe.ac.uk/vsa/

**Table 1.** Log of the spectroscopic observations: dates, Julian dates, exposure times, airmass, seeing, and run number.

| Date | UT | HJD | Exp. (s) | Airmass | Seeing (″) | Run |
|---|---|---|---|---|---|---|
| 07.06.14 | 04:33:15 | 2 456 815.69535 | 3000 | 1.007–1.013 | 0.72–0.84 | 1 |
| 24.06.14 | 01:55:50 | 2 456 832.58620 | 2700 | 1.083–1.026 | 0.47–0.73 | 2 |
| 20.07.14 | 05:13:40 | 2 456 858.72267 | 2700 | 1.329–1.591 | 0.52–0.53 | 3 |
| 30.07.14 | 01:26:09 | 2 456 868.56407 | 2700 | 1.004–1.023 | 0.83–0.75 | 4 |
| 14.08.14 | 01:00:33 | 2 456 883.54517 | 2750 | 1.010–1.047 | 0.71–0.69 | 5 |
| 14.08.14 | 01:58:18 | 2 456 883.54517 | 2750 | 1.048–1.126 | 0.64–0.72 | 6 |
| 14.08.14 | 02:45:54 | 2 456 883.61832 | 2750 | 1.129–1.264 | 0.77–1.00 | 7 |

**Fig. 1.** HP 1 $JHK_s$-combined colour image from the VVV survey. The image has size of $2 \times 2$ arcmin$^2$. North is at 45° anticlockwise.

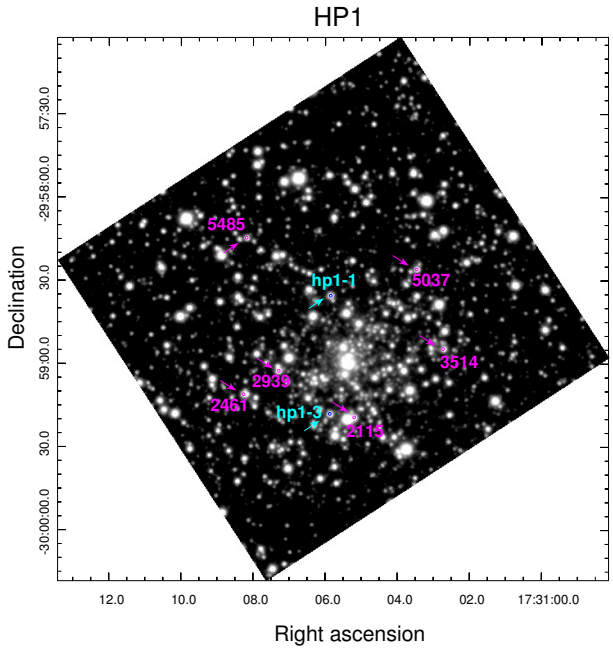


**Fig. 2.** $z$ image from the VVV survey, indicating the location of the sample stars.

Figure 3 shows the $V, I$ CMD of HP 1 and the location of the program stars on the red giant branch.

## 3. Photometric stellar parameters

### 3.1. Temperatures

The selected stars, their ID and 2MASS designations, coordinates, $V, I$ magnitudes from Ortolani et al. (1997), and the 2MASS $JHK_s$ (Skrutskie et al. 2006)[2] and VVV $JHK_s$ magnitudes (Saito et al. 2012) are listed in Table 3. These magnitudes and colors were used to derive initial estimates of the effective temperature and gravity, which were fine-tuned with spectroscopic data using the Fe I and Fe II lines (see Sect. 4).

For star 2461, the identification in the VVV images seems to indicate a blend of at least three stars, as can be seen in Fig. 4. The VVV reductions were made in aperture photometry, which does not yield reliable magnitudes in this case. Only PSF photometry, which is being carried out by the VVV group, will allow distinguishing such cases. For the spectroscopy, the size of 1 arcsec of the fiber does allow observing the correct star.

The reddening value of $E(B-V) = 1.19$ was derived from $V, I$ CMDs by Ortolani et al. (1997). Barbuy et al. (1998) adopted

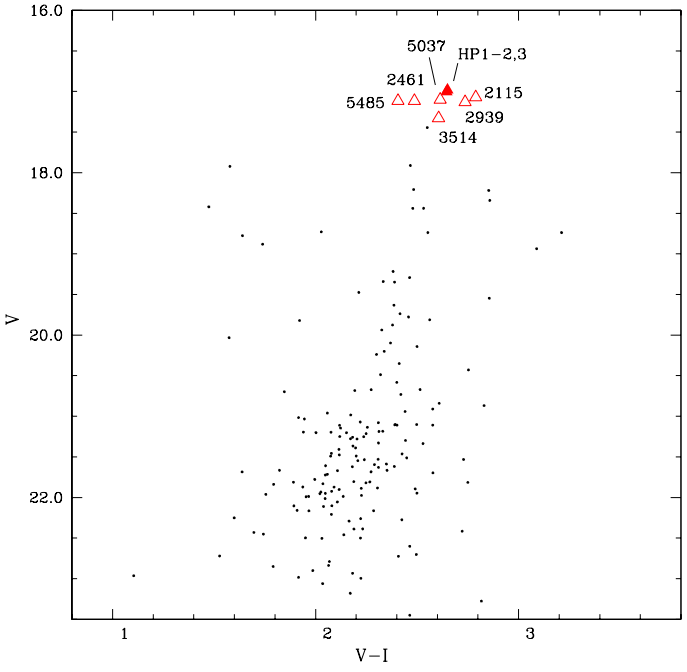


**Fig. 3.** $V, I$ CMD of HP 1 based on data from Ortolani et al. (1997), with the $V, V-I$ of the sample stars indicated.

[2] http://ipac.caltech.edu/2mass/releases/allsky/

**Table 2.** Radial velocities of the UVES sample stars in each of the seven exposure runs, corresponding heliocentric radial velocities, and mean heliocentric radial velocity.

| Target | $v_r^{obs}$ | $v_r^{hel.}$ | Target | $v_r^{obs}$ | $v_r^{hel.}$ |
|---|---|---|---|---|---|
| | km s$^{-1}$ | km s$^{-1}$ | | km s$^{-1}$ | km s$^{-1}$ |
| 2115 1 | +37.024 | +41.004 | 2461 1 | +36.430 | +40.41 |
| 2115 2 | +45.313 | +41.143 | 2461 2 | +44.920 | +40.75 |
| 2115 3 | +57.650 | +41.140 | 2461 3 | +57.695 | +41.185 |
| 2115 4 | +60.847 | +40.797 | 2461 4 | +61.178 | +41.128 |
| 2115 5 | +65.612 | +40.812 | 2461 5 | +65.902 | +41.102 |
| 2115 6 | +65.699 | +40.799 | 2461 6 | +65.995 | +41.095 |
| 2115 7 | +65.819 | +40.839 | 2461 7 | +66.137 | +41.157 |
| Mean | – | +41.006 | Mean | – | +41.048 |
| 2939 1 | +41.756 | +45.736 | 3514 1 | +31.695 | +35.675 |
| 2939 2 | +50.289 | +46.119 | 3514 2 | +39.904 | +35.734 |
| 2939 3 | +62.512 | +46.002 | 3514 3 | +52.524 | +36.014 |
| 2939 4 | +66.057 | +46.007 | 3514 4 | +55.573 | +35.523 |
| 2939 5 | +70.718 | +45.918 | 3514 5 | +59.992 | +35.192 |
| 2939 6 | +70.859 | +45.959 | 3514 6 | +60.104 | +35.204 |
| 2939 7 | +70.974 | +45.994 | 3514 7 | +60.168 | +35.188 |
| Mean | | +46.035 | Mean | – | +35.577 |
| 5037 1 | +37.355 | +41.335 | 5485 1 | +30.851 | +34.831 |
| 5037 2 | +45.627 | +41.457 | 5485 2 | +38.234 | +34.064 |
| 5037 3 | +58.229 | +41.719 | 5485 3 | +50.745 | +34.235 |
| 5037 4 | +61.994 | +41.994 | 5485 4 | +54.665 | +34.615 |
| 5037 5 | +66.700 | +41.900 | 5485 5 | +59.565 | +34.765 |
| 5037 6 | +66.684 | +41.784 | 5485 6 | +59.782 | +34.882 |
| 5037 7 | +66.978 | +41.998 | 5485 7 | +59.832 | +34.852 |
| Mean | | +41.807 | Mean | – | +34.679 |

$E(B-V) = 1.21$ by using a slightly different $R_V$ value. Barbuy et al. (2006) reported previous literature extinction values, and based on a reanalysis of CMD data, adopted $E(B-V) = 1.12$. Ortolani et al. (2011) adopted $E(V-K) = 3.33$, which translates into $E(B-V) = 1.21$ using $E(V-K)/E(B-V) = 2.744$ (Rieke & Lebofsky 1985); the use of a different reddening law does not affect the result much. In the present work we adopted $E(B-V) = 1.12$, following Barbuy et al. (2006).

Effective temperatures were derived from $V-I$, $V-K$, and $J-K$ using the color-temperature calibrations of Alonso et al. (1999, hereafter AAM99). These relations are similar to those by Ramirez & Meléndez (2005), as shown in their Fig. 11. The advantage of using the calibrations of Alonso et al. is that the bolometric corrections can be calculated, despite the disadvantage of having to translate Cousins to Johnson I, and 2MASS to TCS $JHK$ colors. To translate $V-I$ from the Cousins to the Johnson system, we adopted $(V-I)_C = 0.778(V-I)_J$ (Bessell 1979). The $J, H, K_S$ 2MASS magnitudes and colors were translated from the 2MASS system to CIT (California Institute of Technology), and from this to TCS (Telescopio Carlos Sánchez), using the relations from Alonso et al. (1998). The VVV $JHK_s$ colors were translated into the 2MASS $JHK_s$ system, using relations reported by Soto et al. (2013). The derived photometric effective temperatures are listed in Table 4.

### 3.2. Gravities

The gravity values were computed using the classical formula

$$\log g_* = 4.44 + 4\log\frac{T_*}{T_\odot} + 0.4(M_{bol*} - M_{bol\odot}) + \log\frac{M_*}{M_\odot}.$$

We adopted $T_\odot = 5770$ K and $M_{bol\odot} = 4.75$ for the Sun and $M_* = 0.85\,M_\odot$ for the red giant branch (RGB) stars. For HP 1 we assumed a distance modulus of $(m-M)_0 = 14.15$ (Ortolani et al. 1997, 2011), and the gravities were computed and are reported in Table 4. Bolometric corrections were computed with formulae by AAM99. The photometric gravity values were computed assuming the bolometric corrections from the temperature $T(V-I)$ values (Col. 9), and also with the spectroscopic temperature values (Col. 11). The final spectroscopic gravities, described in the next section, are given in Col. 12 of Table 4, and are compatible with the photometric gravities.

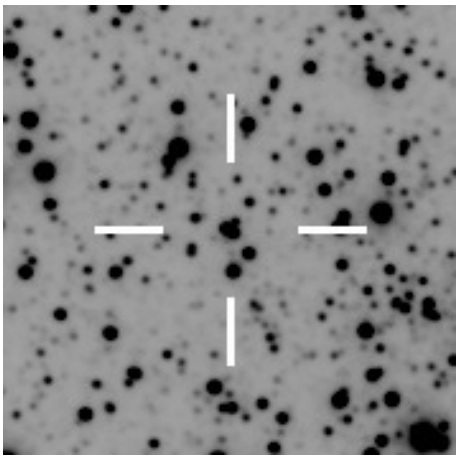

**Fig. 4.** Image of star 2461 in the VVV survey, indicating a blend of stars. Extraction of ~20 arcsec. North is 45° anticlockwise.

## 4. Spectroscopic stellar parameters

The equivalent widths (EW) were measured using the automatic code DAOSPEC, developed by Stetson & Pancino (2008). We also measured EWs line by line using IRAF for a few lines, in particular for Fe II. The EWs measured for the Fe I and Fe II lines are reported in Table A.1. We limited EWs to $20 < EW(\text{mÅ}) < 99$ to avoid on one hand, too weak lines that are affected by the continuum level choice, in particular when using software such as DAOSPEC, and on the other hand, the saturated lines that are less sensitive to abundance variations.

In Fig. 5 we show the computed Fe II lines compared with the observed spectra. Given the blends in lines Fe II 6084.11 and 6456.39 Å, these lines were not used.

In the line list given in Table A.1, literature oscillator strengths for Fe I from NIST[3] and VALD3[4] databases (Martin et al. 2002; Piskunov et al. 1995) are reported. We also give the adopted values, where we have given preference to NIST over VALD. For Fe II we report the log $gf$ values from Fuhr & Wiese (2006) and Meléndez & Barbuy (2009) in Table A.1. We adopted the latter values.

Photospheric 1D models for the sample giants were extracted from the MARCS model atmosphere grid (Gustafsson et al. 2008). We adopted the spherical and mildly CN-cycled set ([C/Fe] = −0.13, [N/Fe] = +0.31). This choice is due to the well-known mixing that occurs along the RGB, which transforms C into N. These models consider [$\alpha$/Fe] = +0.20 for [Fe/H] = −0.50 and [$\alpha$/Fe] = +0.40 for [Fe/H] ≤ −1.00. The LTE abundance analysis and the spectrum synthesis calculations were performed using the code described in Barbuy et al. (2003) and Coelho et al. (2005). An Fe abundance of

[3] http://physics.nist.gov/PhysRefData/ASD/lines_form.html
[4] http://vald.astro.univie.ac.at/~vald3/php/vald.php

**Table 3.** Identifications, coordinates, $V, I$ magnitudes from Ortolani et al. (1997), and $JHK_s$ magnitudes from the 2MASS and VVV surveys.

| ID no. | 2MASS ID | $\alpha_{2000}$ | $\delta_{2000}$ | $V$ | $I$ | $J$ | $H$ | $K_s$ | $J_{VVV}$ | $H_{VVV}$ | $K_{VVV}$ |
|---|---|---|---|---|---|---|---|---|---|---|---|
| 2115 | – | 17:31:05.420 | −29:59:20.71 | 17.070 | 14.281 | – | – | – | – | – | – |
| 2461 | 17310822–2959108 | 17:31:08.22 | −29:59:10.85 | 17.115 | 14.628 | – | – | – | 12.066[a] | 10.249[a] | 10.959[a] |
| 2939 | 17310729–2959021 | 17:31:07.31 | −29:59:02.30 | 17.131 | 14.394 | 11.901 | 10.869 | 10.595 | – | – | – |
| 3514 | 17310273–2958544 | 17:31:02.74 | −29:58:54.74 | 17.327 | 14.721 | 12.447 | 11.574 | 11.212 | – | 11.248 | 11.378 |
| 5037 | 17310347–2958259 | 17:31:03.48 | −29:58:26.04 | 17.101 | 14.487 | 12.302 | 11.303 | 10.994 | 12.287 | 11.502 | 11.115 |
| 5485 | 17310817–2958147 | 17:31:08.19 | −29:58:14.81 | 17.116 | 14.710 | 12.761 | 11.965 | 11.364 | 12.737 | 11.989 | 11.729 |
| hp1-2 | 17310585–2958354 | 17:31:05.852 | −29:58:35.5 | 16.982 | 14.332 | 12.21 | 11.268 | 10.969 | 12.1527 | 11.4164 | 11.0541 |
| hp1-3 | 17310587–2959180 | 17:31:05.872 | −29:59:18.1 | 17.003 | 14.358 | 12.167 | 11.146 | 10.828 | 12.1220 | 10.9702 | 10.9119 |

**Notes.** The two stars analyzed in Barbuy et al. (2006) are also listed. [(a)] Identification of star 2461 in VVV may be a blend of stars.

**Table 4.** Photometric stellar parameters derived using the calibrations by Alonso et al. (1999) for $V-I$, $V-K$, $J-K$, bolometric corrections computed by adopting the $V, I$ derived temperature, bolometric magnitudes, and corresponding gravity log $g$, and final spectroscopic parameters.

| | Photometric parameters | | | | | | | | Spectroscopic parameters | | | | | | | |
|---|---|---|---|---|---|---|---|---|---|---|---|---|---|---|---|---|
| star | $T_{V-I}$ | $T_{V-K}$ | $T_{J-K}$ | $T_{V-K}$ | $T_{J-K}$ | BC$_V$ | $M_{bol}$ | log $g$ | $T_{eff}$ | BC$_V$ | log $g$ | log $g$ | [FeI/H] | [FeII/H] | [Fe/H] | $v_t$ |
| | | 2MASS | | VVV | | | | | | | | | | | | |
| | (K) | (K) | (K) | (K) | (K) | | | | (K) | | | | | | | km s$^{-1}$ |
| 2115 | 4196.6 | – | – | – | – | −0.702 | −0.18 | 1.95 | 4530 | −0.457 | 1.99 | 2.00 | −0.98 | −1.02 | −1.00 | 1.45 |
| 2461 | 4735.2 | – | – | 4217.9 | 4506.5 | −0.368 | −0.14 | 2.04 | 4780 | −0.323 | 2.04 | 2.05 | −1.13 | −1.09 | −1.11 | 1.90 |
| 2939 | 4274.4 | 4025.1 | 4423.3 | – | – | −0.638 | −0.12 | 1.98 | 4525 | −0.440 | 2.01 | 2.00 | −1.07 | −1.07 | −1.07 | 1.55 |
| 3514 | 4496.6 | 4249.4 | 4624.0 | 4855.9 | – | −0.487 | 0.08 | 2.09 | 4590 | −0.349 | 2.06 | 2.00 | −1.18 | −1.19 | −1.18 | 1.90 |
| 5037 | 4481.9 | 4254.3 | 4418.0 | 4324.0 | 4576.4 | −0.496 | −0.15 | 1.99 | 4570 | −0.429 | 2.05 | 2.15 | −0.98 | −1.03 | −1.0 | 1.20 |
| 5485 | 4920.4 | 4499.6 | 4197.0 | 4812.7 | 5152.4 | −0.298 | 0.14 | 2.08 | 4920 | −0.282 | 2.09 | 2.07 | −1.18 | −1.18 | −1.18 | 1.80 |

**Notes.** A reddening of $E(B-V) = 1.12$ is assumed. For each star the last columns give the spectroscopic parameters from UVES spectra (present work).

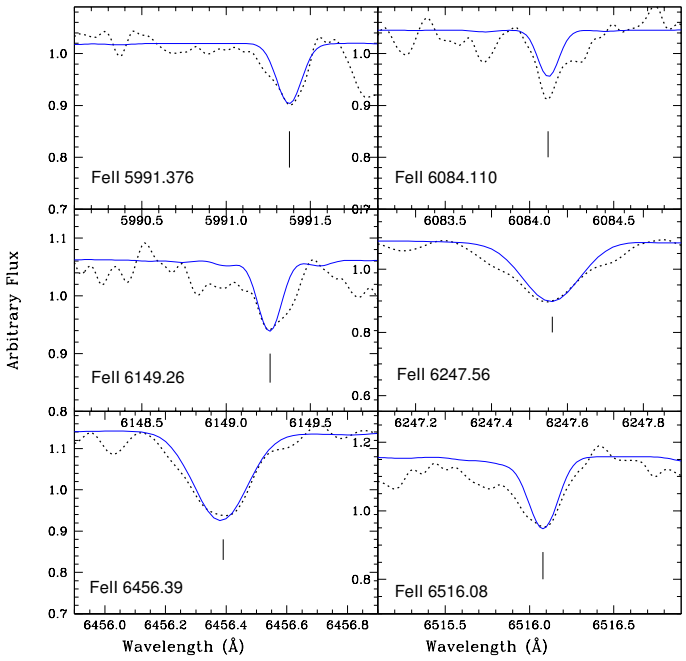


**Fig. 5.** FeII lines for star 5037. Dotted lines: observed spectra. Blue solid lines: synthetic spectra.

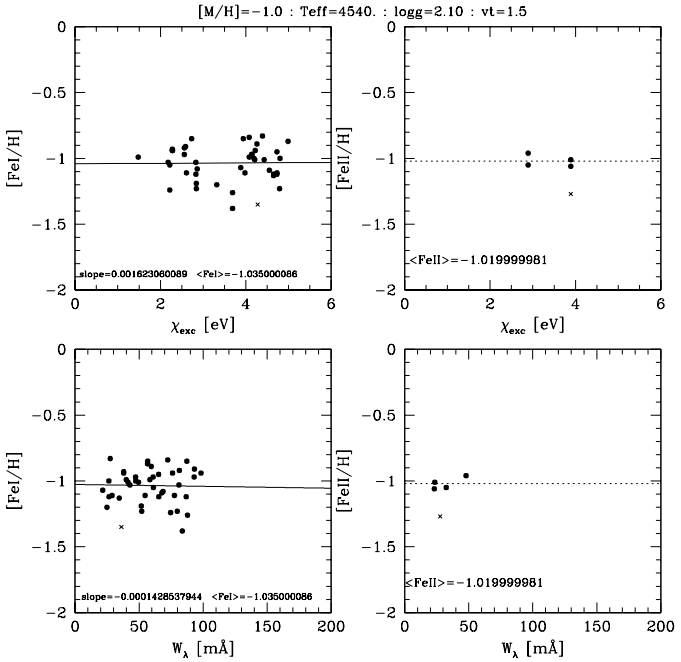


**Fig. 6.** Excitation and ionization equilibria of Fe I and Fe II lines for star 2939.

$\epsilon$(Fe) = 7.50 (Grevesse & Sauval 1998) was adopted. Molecular lines of MgH ($A^2\Pi$-$X^2\Sigma$), CN ($A^2\Pi$-$X^2\Sigma$), $C_2$ Swan ($A^3\Pi$-$X^3\Pi$), TiO ($A^3\Phi$-$X^3\Delta$) $\gamma$ and TiO ($B^3\Pi$-$X^3\Delta$) $\gamma$' systems are taken into account.

The stellar parameters were derived by initially adopting the photometric effective temperature and gravity, and then by further constraining the temperature by imposing excitation equilibrium for Fe I lines. Fe I and Fe II lines allowed deriving gravities by imposing ionization equilibrium. Microturbulence velocities $v_t$ were determined by canceling the trend of Fe I abundance vs. equivalent width.

The final spectroscopic parameters $T_{eff}$, log $g$, [Fe I/H], [Fe II/H], [Fe/H], and $v_t$ values are reported in the last columns of Table 4. An example of excitation and ionization equilibria using Fe I and Fe II lines is shown in Fig. 6 for star HP1-2939.

**Table 5.** Carbon, nitrogen, and oxygen abundances derived from $C_2$ (0,1), CN (5,1), and [OI] lines.

| Line | $\lambda$ (Å) | 2115 | 2641 | 2939 | 3514 | 5037 | 5485 |
|---|---|---|---|---|---|---|---|
| $C_2$(0,1) | 5635.5 | ≤+0.0 | ≤+0.0 | ≤+0.0 | ≤+0.0 | ≤+0.0 | ≤+0.0 |
| CN(5,1) | 6332.2 | ≤+0.7 | ≤+0.5 | ≤+0.5 | ≤+0.8 | ≤+0.5 | ≤+0.5 |
| [OI] | 6300.3 | +0.4 | +0.5 | +0.5 | +0.4 | +0.35 | +0.4 |

## 5. Abundance ratios

Abundance ratios were obtained by means of line-by-line spectrum synthesis calculations compared to the observed spectra for the line lists given in Tables 5, B.1–B.3. The fits were made by eye using a series of calculations for different abundances and verifying the continua over 20 Å. We then zoomed and fine-tuned them locally. The solar abundances were adopted from Grevesse et al. (1998), which are close to the latest values by Asplund et al. (2009), Grevesse et al. (2014) or Lodders (2009). For oxygen we adopted $\epsilon$(O) = 8.77 following Allende Prieto et al. (2001) for 1D model atmospheres, which is very close to the value of $\epsilon$(O) = 8.76 recommended from 3D models by Steffen et al. (2015).

### 5.1. Carbon, nitrogen, and oxygen

The carbon abundances were estimated from the $C_2$(0,1) bandhead at 5635.3 Å. The list of laboratory $C_2$ lines (Phillips & Davis 1968) was reported in Barbuy et al. (2014). Because the feature is weak in these metal-poor stars, we adopted [C/Fe] = 0.0 and just checked that this was a suitable upper limit. The nitrogen abundances were measured using the CN (5, 1) 6332.18 Å of the CN $A^2\Pi$-$X^2\Sigma$ red system. The CN feature is also weak, but can be used to estimate a reliable upper limit for the *N* abundance.

The forbidden oxygen [OI] 6300.311 Å line was used to derive the oxygen abundances. A check for telluric lines was carried out by overplotting the spectrum of a fast-rotation B star, and we verified that none of the stars were affected by them. The resulting C, N, and O abundances are given in Table 5, showing the essentially adopted carbon abundance of [C/Fe] ∼ 0.0, the enhanced nitrogen abundances as expected in giants, and enhanced oxygen abundances of +0.35 < [O/Fe] < +0.5, typical of enrichment by SNII.

### 5.2. Odd-Z elements Na, Al, and alpha-elements

In Tables B.1 and B.2 we report the line-by-line abundances of the odd-Z elements Na, Al, and the alpha-elements Mg, Si, Ca, and Ti abundances. We have inspected the abundance results as a function of effective temperature and microturbulence velocity and found no trend for any of the elements. In addition to the six sample stars, we also rederived the abundances of Na, Al and Mg for the two stars analyzed in Barbuy et al. (2006), as given in Table 6.

### 5.3. Heavy elements

In Table B.3 we report the line-by-line derivation of abundances for lines of the neutron-capture dominant s-elements Sr, Y, Zr, La, Ba, and the *r*-element Eu. As in Table B.1, we also rederived the abundances of heavy elements for the two stars analyzed in Barbuy et al. (2006). The hyperfine structure (HFS) for the studied lines of La II, Ba II and Eu II were taken into account, as described in Barbuy et al. (2014). The fits to the lines of Eu II 6645, Ba II 6141 and Ba II 6496 Å lines in star 2115 are shown in Fig. 8.

**Table 6.** Abundance uncertainties for star 2115 for uncertainties of $\Delta T_{\rm eff}$ = +100 K, $\Delta\log g$ = +0.2, $\Delta v_{\rm t}$ = 0.2 km s$^{-1}$, an assumed error in EWs or continuum placement, and the corresponding total error.

| Abundance | $\Delta T$ 100 K | $\Delta\log g$ 0.2 dex | $\Delta v_t$ 0.2 kms$^{-1}$ | $EW$ | $(\sum x^2)^{1/2}$ |
|---|---|---|---|---|---|
| (1) | (2) | (3) | (4) | (5) | |
| [FeI/H] | +0.06 | +0.03 | −0.07 | 0.02 | 0.10 |
| [FeII/H] | −0.12 | +0.11 | −0.03 | 0.02 | 0.17 |
| [N/Fe] | −0.05 | +0.00 | +0.00 | 0.10 | 0.11 |
| [O/Fe] | +0.00 | −0.05 | +0.00 | 0.05 | 0.07 |
| [NaI/Fe] | +0.10 | +0.00 | −0.01 | 0.10 | 0.14 |
| [Al/Fe] | +0.05 | +0.00 | +0.00 | 0.10 | 0.11 |
| [MgI/Fe] | +0.03 | +0.00 | +0.00 | 0.10 | 0.10 |
| [SiI/Fe] | +0.00 | +0.02 | −0.02 | 0.05 | 0.06 |
| [CaI/Fe] | +0.10 | +0.00 | −0.05 | 0.05 | 0.12 |
| [TiI/Fe] | +0.10 | +0.00 | −0.03 | 0.05 | 0.12 |
| [TiII/Fe] | −0.10 | +0.08 | −0.01 | 0.05 | 0.14 |
| [SrI/Fe] | −0.15 | +0.00 | +0.00 | 0.20 | 0.25 |
| [YI/Fe] | −0.15 | +0.00 | +0.00 | 0.10 | 0.18 |
| [YII/Fe] | +0.02 | −0.15 | +0.00 | 0.10 | 0.18 |
| [ZrI/Fe] | −0.20 | +0.00 | +0.00 | 0.10 | 0.22 |
| [BaII/Fe] | +0.02 | +0.02 | −0.20 | 0.10 | 0.23 |
| [LaII/Fe] | +0.00 | +0.03 | +0.00 | 0.10 | 0.10 |
| [EuII/Fe] | +0.00 | +0.03 | +0.00 | 0.10 | 0.10 |

**Notes.** The errors correspond to the difference in abundance obtained with the modified parameters.

### 5.4. Errors

The errors due to uncertainties in spectroscopic parameters are given in Table 6, applied to the sample star HP 1: 2115. The error on the slope in the FeI vs. excitation potential implies an error in the temperature of ±100 K for the sample stars. An uncertainty of the order of 0.2 km s$^{-1}$ on the microturbulence velocity is estimated from the imposition of a constant value of [Fe/H] as a function of EWs. Errors based on EWs are given on FeI and FeII abundances.

The errors on the abundance ratios [X/Fe] were computed by fitting the lines with the modified atmospheric model. The error reported corresponds to the new value obtained by using the modified model atmosphere. The element abundance ratios, induced by a change of $\Delta T_{\rm eff}$ = +100 K, $\Delta\log g$ = +0.2, $\Delta v_{\rm t}$ = 0.2 km s$^{-1}$, and a total error estimate, are given in Table 6. These errors are overestimated because the stellar parameters are covariant. The correlation matrix is difficult to estimate, however, and would add other error sources, so that we preferred the quadratic sum of the diagonal terms as reliable.

Additionally, an uncertainty of about 0.8 mÅ in the EWs of the Fe lines was estimated with the formula of (Cayrel 1988, 2004). With a mean $FWHM$ = 12.5 pixels, or 0.184 Å, a CCD pixel size of 15 $\mu$m, or $\delta x$ = 0.0147 Å in the spectra, and assuming a mean $S/N$ = 100, we obtain an error $\Delta EW$ ∼ 0.8 mÅ.

We derived abundances uniquely from fitting synthetic spectra, such that we need to take the uncertainty in the continuum placement into account. We estimate an error of 0.1 dex for the weak and strong lines and 0.05 dex for medium lines. This is included in Table 6.

**Table 7.** Mean abundances of C, N, odd-Z elements Na, Al, $\alpha$-elements O, Mg, Si, Ca, Ti, and heavy elements Y, Sr, Zr, Ba, La, and Eu.

| [X/Fe] | 2115 | 2461 | 2939 | 3514 | 5037 | 5485 | HP 1-2 | HP 1-3 | Mean | NGC 6522 |
|---|---|---|---|---|---|---|---|---|---|---|
| C | ≤+0.00 | ≤+0.00 | ≤+0.00 | ≤+0.00 | ≤+0.00 | ≤+0.00 | +0.00 | +0.00 | +0.00 | −0.03 |
| N | ≤+0.70 | +≤0.50 | ≤+0.50 | ≤+0.80 | ≤+0.50 | ≤+0.50 | +0.50 | +0.20 | +0.53 | +0.67 |
| O | +0.40 | +0.50 | +0.50 | +0.40 | +0.35 | +0.40 | +0.30 | +0.30 | +0.40 | +0.36 |
| Na | +0.03 | −0.30 | −0.23 | −0.10 | −0.10 | −0.30 | −0.05 | −0.20 | −0.16 | +0.05 |
| Al | −0.15 | +0.05 | +0.05 | +0.08 | +0.20 | +0.20 | −0.28 | +0.18 | +0.04 | +0.20 |
| Mg | +0.30 | +0.35 | +0.65 | +0.35 | +0.33 | +0.40 | +0.15 | +0.33 | +0.36 | +0.23 |
| Si | +0.25 | +0.31 | +0.33 | +0.31 | +0.20 | +0.15 | +0.30 | +0.30 | +0.27 | +0.13 |
| Ca | +0.28 | +0.11 | +0.21 | +0.11 | +0.26 | +0.04 | −0.04 | +0.10 | +013 | +0.13 |
| TiI | +0.26 | +0.16 | +0.28 | +0.17 | +0.16 | +0.06 | +0.07 | +0.08 | +0.16 | +0.04 |
| TiII | +0.40 | +0.18 | +0.23 | +0.19 | +0.31 | +0.13 | +0.10 | +0.15 | +0.21 | +0.17 |
| Y | +0.15 | +0.30 | +0.25 | +0.35 | +0.10 | +0.50 | -0.15 | −0.1 | +0.18 | +0.31 |
| Zr | +0.15 | −0.10 | +0.28 | +0.37 | +0.20 | +0.15 | – | −0.02 | +0.15 | +0.18 |
| Sr | +0.55: | – | +0.30 | – | +0.40 | – | +0.50: | +0.30: | +0.41: | +0.23 |
| Ba | +0.50 | +0.30 | +0.50 | +0.00 | +0.75 | +0.45 | +0.65 | +0.47 | +0.46 | +0.32 |
| La | +0.33 | +0.23 | +0.43 | +0.32 | +0.08 | +0.10 | −0.15 | −0.18 | +0.23 | – |
| Eu | +0.50 | +0.50 | +0.70 | +0.60 | +0.60 | +0.55 | +0.40 | +0.55 | +0.15 | +0.30 |
| Ba/Eu | 0.0 | −0.20 | −0.20 | −0.60 | +0.15 | −0.10 | +0.25 | −0.08 | +0.31 | – |
| $v_r$ (km s$^{-1}$) | +41.0 | +41.0 | +46.0 | +35.0 | +41.0 | +34.0 | +44.6 | +44.0 | | |

**Notes.** Mean values for NGC 6522 are given in the last column.

## 6. Discussion

In Table 7 we report the mean abundances for each star and for each element, and in the last line we report the radial velocities.

### 6.1. Two stellar populations?

We derived a mean metallicity of [Fe/H] = −1.06 ± 0.15 by adding the two stars previously analyzed in HP 1 by Barbuy et al. (2006).

Two stars, 3514 and 5485, show a slightly lower metallicity of [Fe/H] = −1.18 and, possibly not by coincidence, they also show radial velocities of $v_r^{hel}$ = +35.6 and +34.7 km s$^{-1}$, respectively, which is lower than the radial velocities of the other six stars, whose values lie in the range $-41.0 < v_r^{hel} < -47.0$ km s$^{-1}$. Their radial velocities are compatible with being members within the uncertainties. If these two stars correspond to an earlier stellar generation in the cluster, then we might have a first stellar generation with [Fe/H] = −1.18 and a second generation with a mean metallicity of [Fe/H] = −1.02 ± 0.05, as found for the other six stars.

The membership of these two lower velocity stars is another question. Recent work by Bellini et al. (2015) for NGC 2808 has shown differences in radial velocities between two stellar populations in a cluster. Malavolta et al. (2015) studied M4, showing that it has a dispersion of 4 km s$^{-1}$. HP 1 is probably subject to tidal effects that lead to possible perturbations or even disruption. The two low-velocity stars might become unbound from the cluster, given their difference in velocites of $\Delta v_r^{hel} = -10$ km s$^{-1}$.

### 6.2. Odd-Z elements and Na-O anticorrelation

Na and Al tend to be underabundant in HP 1. This may be due to internal nucleosynthesis (Gratton et al. 2012). In particular, a Na-O anticorrelation due to the Ne-Na cycle of proton capture reactions was shown by Carretta et al. (2009) to be confirmed for several globular clusters. In Fig. 7 we show the [Na/Fe] vs. [O/Fe] for 14 stars of NGC 6121 by Carretta et al. (2009), compared to the present results for HP 1. This figure points to evidence for a Na-O anticorrelation in HP 1, but with the difference

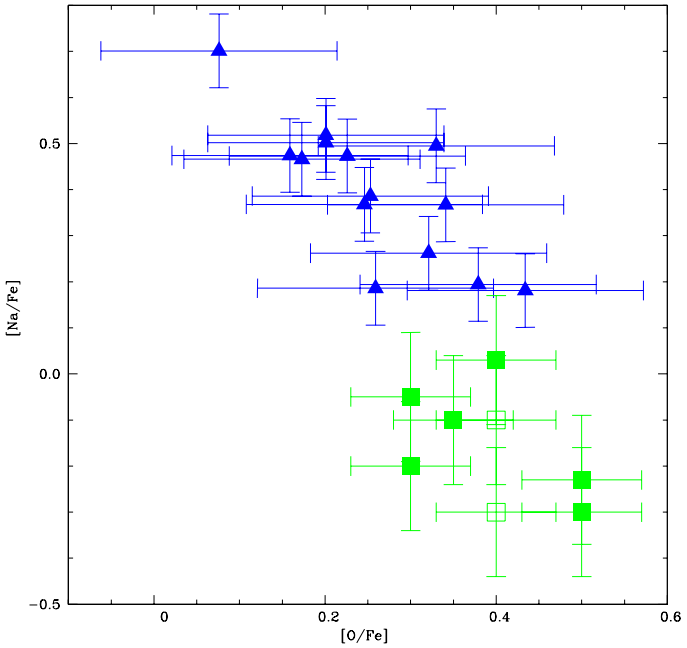


**Fig. 7.** [Na/Fe] vs. [O/Fe] for the sample stars compared with stars of NGC 6121. Symbols: present work: green filled squares: the 6 HP 1 stars with [Fe/H] = −1.0 ± 0.05; open green squares: the 2 HP 1 stars with [Fe/H] = −1.18; compared with blue filled triangles: stars of NGC 6121.

with respect to NGC 6121 and most other clusters studied by Carretta et al. (2009), of Na being lower than in the other clusters. Na is originally probably underabundant in HP 1, which reinforces its peculiar pattern.

### 6.3. Alpha-elements

The $\alpha$-element enhancements in O, Mg, and Si together with the enhancement of the *r*-process element Eu are indicative of a fast early enrichment by SNII. Ca and Ti are only slightly enhanced with [Ca/Fe] = +0.13 and [Ti/Fe] = +0.18 (a mean of Ti I and

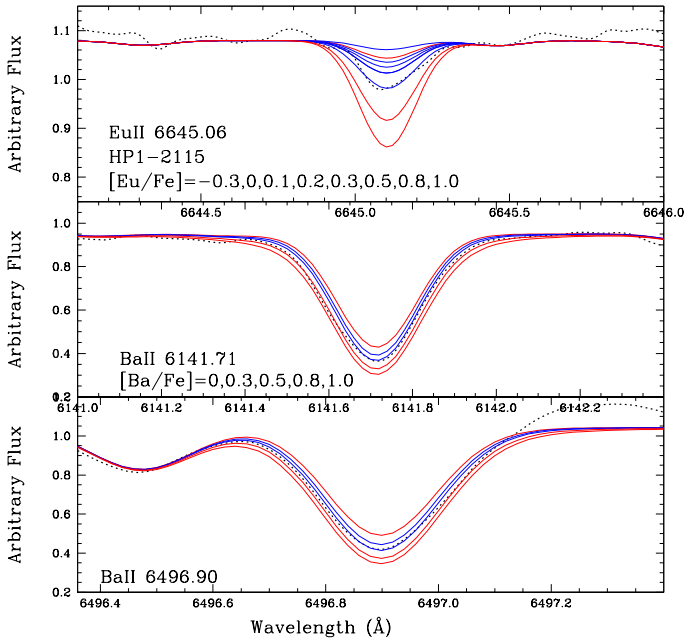


**Fig. 8.** Fits to the Eu II 6645, Ba II 6141 and Ba II 6496 Å lines in star 2115. The [Eu/Fe] and [Ba/Fe] values adopted for the different calculations are indicated in the panels.

Ti II abundances). The difference between O, Mg, and Si on one hand and Ca and Ti on the other was also detected in other bulge samples, such as NGC 6522 (Barbuy et al. 2014). The mean values for NGC 6522 are reported for comparison purposes in Table 10.

The fact that [O, Mg, Si/Fe] are higher than [Ca, Ti/Fe] does not match the results for field stars by González et al. (2011). This might be explained by the mass of supernovae type II that enriched the cluster, or else by the absence of contribution from supernovae type I.

### 6.4. Heavy elements

Figure 9 shows the results for Y, Zr, Ba, La, and Eu compared to other available heavy element abundance determinations in bulge stars. The Sr abundances are not very reliable because the lines used are extremely faint. We therefore did not plot this element. Literature data include a) field red giants in Plaut's field analyzed by Johnson et al. (2012); b) seven red giants in the globular cluster M62 (NGC 6266) by Yong et al. (2014); c) microlensed bulge dwarf stars analyzed by Bensby et al. (2013); d) four red giants in NGC 6522 analyzed by Barbuy et al. (2014); e) 56 bulge field red giants for which Van der Swaelmen et al. (2016) derived heavy element abundances; and f) five bulge field red giants with [Fe/H] $\approx -1.0$ from the sample by Ness et al. (2013) that were analyzed by Siqueira-Mello et al. (2016).

This figure shows that [Zr/Fe], [Ba/Fe], [La/Fe], and [Eu/Fe] increase steadily with decreasing metallicity. At a metallicity of around [Fe/H] $\approx -1.0$, the dominantly s-elements Y, Zr, Ba, and La show an abundance spread. This behavior is compatible with expectations from massive spinstars: a spread like this is predicted from the models by Frischknecht et al. (2016, and references therein) and Meynet et al. (2016, and references therein), as discussed and shown in Chiappini et al. (2011), Chiappini (2013), and Barbuy et al. (2014).

On the other hand, the enhancements of O, Mg, and Eu, and to a lesser extent of Si, Ca, and Ti, indicate an early enrichment by supernovae type II. The small fraction of *r*-process production of the dominantly s-elements in the solar neighborhood might be responsible for their production at early times, as first suggested by Truran (1981). To verify the *r*- or *s*-nature of the heavy element abundances, we report the [Ba/Eu] ratios in penultimate line of Table 7.

The ratio [Ba/Eu] is indicative of the relative contribution of the *s*- and *r*-process. We find $-0.60 <$ [Ba/Eu] $< +0.25$, and $[\mathrm{Ba/Eu}]_r \sim -0.8$ is given as typical of a pure *r*-process by Bisterzo et al. (2014). This means that the barium-to-europium ratio is above the line for a pure *r*-process and might be interpreted as due to an *s*-process. The *s*-process can be due to transfer of matter from an AGB companion or to a general AGB pollution, as recently made likely to occur in multi-population clusters (e.g. Renzini et al. 2015), or to spinstars. The spread in abundances of Y, Sr, Zr, Ba, and La at around [Fe/H] $\sim -1.0$ is the main indicator of the contribution by spinstars (Chiappini et al. 2011). Finally, both *r*- and *s*- processes may take place, that is, massive spinstars producing *s*-elements may not exclude a later explosion of the supernova and the subsequent r-process. Another possible explanation would be an additional process that enhanced the lightest heavy elements at early times. Several models are proposed in the literature, such as the lighter element primary process LEPP. Travaglio et al. (2004) discussed this process for the Sun. A different LEPP mechanism was discussed by Montes et al. (2007) for metal-poor stars. A possible explanation for the LEPP is the weak r-process (Wanajo & Ishimaru 2006) or supernovae neutrino-driving winds (Arcones & Thielemann 2013). We note that different processes might be enriching in Y, Sr, and Zr at different metallicities and environments. Niu et al. (2015) proposed a unified solution. Finally, it is important to mention that, as pointed out by Roederer et al. (2010; see his Fig. 11), there are varying degrees of enrichment of first- and second-peak elements in stars enriched by neutron capture.

## 7. Conclusions

We carried out a detailed analysis of six red giants of the bulge moderately metal-poor globular cluster HP 1 and added two other previously analyzed stars. A metallicity of [Fe/H] $= -1.06 \pm 0.15$ was derived from the eight stars, and since HP 1 has a blue horizontal branch, this combination of characteristics is an indication of a very old age.

We found overabundances of the $\alpha$-elements [Mg/Fe] $\approx$ [O/Fe] $\approx +0.4$ and [Si/Fe] $\approx +0.3$ and lower values of [Ca/Fe] $\approx$ [Ti/Fe] $\approx +0.10$. The light odd-Z elements Na and Al are low with [Na/Fe] $= -0.20$ and [Al/Fe] $= +0.18$. In particular, because of the low Na abundance, the Na-O anticorrelation is unclear. HP 1 has a relatively low mass, with absolute magnitude $M_V = -6.46$, therefore it is probably less prone to show this effect, as demonstrated for several clusters by Carretta et al. (2009).

The dominantly s-elements are moderately enhanced with [Ba/Fe] $\approx +0.32$ and the r-element [Eu/Fe] $\approx +0.30$. These values are very similar to the results for NGC 6522 (Barbuy et al. 2014), indicating that these two clusters that are located in the central parts of the Galactic bulge may be of similar origin.

The abundances in the earliest globular clusters can reveal the nature of the first stars and also the location at which they formed in the Galaxy. It appears to be of great importance to further investigate this and other such clusters in terms of metallicity, abundances, kinematics, orbits, and ages.

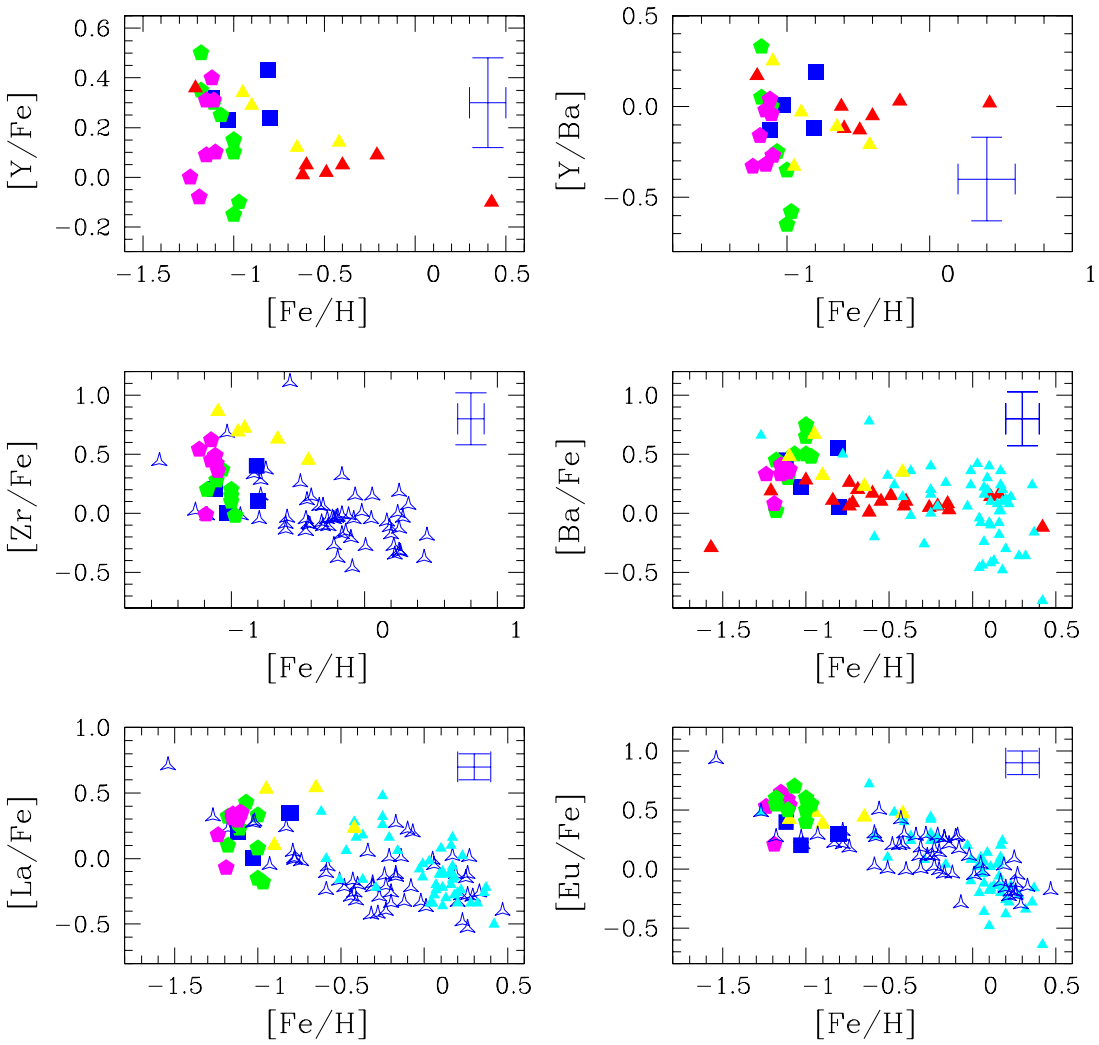


**Fig. 9.** [Y, Zr, Ba, La, Eu/Fe] vs. [Fe/H] and [Y/Ba] vs. [Fe/H] for the sample stars compared with literature values. Symbols: blue filled squares: NGC 6522; magenta pentagons: M62; red filled triangles: bulge field dwarfs by Bensby et al. (2013); blue triangles: bulge field red giants from Rich et al. (2012); cyan triangles: Van der Swaelmen et al. (2016); yellow triangles: Siqueira-Mello et al. (2016); green filled pentagons: HP 1 from the present work.

*Acknowledgements.* B.B., E.C., A.V., C.S.M., H.E., and E.B. acknowledge grants and fellowships from CNPq, Capes and Fapesp. S.O. acknowledges the financial support from the Università di Padova and from the Italian Ministero dell'Università e della Ricerca Scientifica e Tecnologica (MURST), Italy. D.M. and M.Z. acknowledge support from the BASAL Center for Astrophysics and Associated Technologies PFB-06, the Ministry of Economy, Development, and Tourism's Millennium Science Initiative through grant IC120009, awarded to The Millennium Institute of Astrophysics (MAS), and Proyectos Fondecyt Regular 1130196 and 1150345.

## References

Allende Prieto, C., Lambert, D. L., & Asplund, M. 2001, ApJ, 556, L63
Alonso, A., Arribas, S., & Martínez-Roger, C. 1998, A&AS, 131, 209
Alonso, A., Arribas, S., & Martínez-Roger, C. 1999, A&AS, 140, 261 (AAM99)
Arcones, A., & Thielemann, F.-K. 2013, J. Phys. G: Nucl. Part. Phys., 40, 013201
Asplund, M., Grevesse, N., Sauval, A. J., & Scott, P. 2009, ARA&A, 47, 481
Ballester, P., Modigliani, A., Boitquin, O., et al. 2000, The Messenger, 101, 31
Barbuy, B., Bica, E., & Ortolani, S. 1998, A&A, 333, 117
Barbuy, B., Perrin, M.-N., Katz, D., et al. 2003, A&A, 404, 661
Barbuy, B., Zoccali, M., Ortolani, S., et al. 2006, A&A, 449, 349
Barbuy, B., Zoccali, M., Ortolani, S., et al. 2007, AJ, 134, 1613
Barbuy, B., Zoccali, M., Ortolani, S., et al. 2009, A&A, 507, 405
Barbuy, B., Chiappini, C., Cantelli, E., et al. 2014, A&A, 570, A76
Bellini, A., Vesperini, E., Piotto, G., et al. 2015, ApJ, 810, L13
Bensby, T., Yee, J. C., Feltzing, S., et al. 2013, A&A, 549, A147
Bessell, M. S. 1979, PASP, 91, 589
Bica, E., Ortolani, S., & Barbuy, B. 2016, PASA, in press [arXiv:1510.07834]
Bisterzo, S., Travaglio, C., Gallino, R., et al. 2014, ApJ, 787, 10
Carpenter, J. M. 2001, AJ, 121, 2851
Carretta, E., Bragaglia, A., Gratton, R., & Lucatello, S. 2009, A&A, 505, 139
Cayrel, R. 1988, in The Impact of Very High S/N Spectroscopy on Stellar Physics, eds. G. Cayrel de Strobel, & M. Spite, IAU Symp., 132, 345
Cayrel, R., Depagne, E., Spite, M., et al. 2004, A&A, 416, 1117
Cescutti, G., & Chiappini, C. 2014, A&A, 565, A51
Cescutti, G., Matteucci, F., Lanfranchi, G. A., & McWilliam, A. 2008, A&A, 491, 401
Cescutti, G., Chiappini, C., Hirschi, R., Meynet, G., & Frischknecht, U. 2013, A&A, 553, A51
Chiappini, C. 2013, Astron. Nachr., 334, 595
Chiappini, C., Hirschi, R., Meynet, G., et al. 2006, A&A, 449, L27
Chiappini, C., Frischknecht, U., Meynet, G., et al. 2011, Nature, 472, 454 (C11)
Coelho, P., Barbuy, B., Meléndez, J., Schiavon, R. P., & Castilho, B. V. 2005, A&A, 443, 735
Davidge, T. J. 2000, ApJS, 126, 105
Dean, J. F., Warpen, P. R., & Cousins, A. J. 1978, MNRAS, 183, 569
Dékány, I., Minniti, D., Catelan, M., et al. 2013, ApJ, 776, L19
Dekker, H., D'Odorico, S., Kaufer, A., Delabre, B., & Kotzlowski, H. 2000, SPIE, 4008, 534D
Dias, B., Barbuy, B., Saviane, I., et al. 2016, A&A, 590, A9
Dufay, J., Berthier, P., & Morignat, B. 1954, Publications of the Observatoire de Haute-Provence, 3, 17
Frischknecht, U., Hirschi, R., & Thielemann, F.-K. 2012, A&A, 538, L2
Frischknecht, U., Hirschi, R., Pignatari, M., et al. 2016, MNRAS, 456, 1803
García-Perez, A., Cunha, K., Shetrone, M., et al. 2013, ApJ, 767, L9

Gran, F., Minniti, D., Saito, R. K., et al. 2016, in press, DOI: 10.1051/0004-6361/201527511
Gratton, R. G., Carretta, E., & Bragaglia, A. 2012, A&ARv, 20, 50
Grevesse, N., & Sauval, J. N. 1998, Space Sci. Rev., 35, 161
Grevesse, N., Asplund, M., Scott, P., & Sauval, A. J. 2015, A&A, 573, A27
Gonzalez, O. A., Rejkuba, M., Zoccali, M., et al. 2011, A&A, 530, A54
Gustafsson, B., Edvardsson, B., Eriksson, K., et al. 2008, A&A, 486, 951
Hekker, S., Snellen, I. A. G., Aerts, C., et al. 2008, A&A, 480, 215
Hill, V., Lecureur, A., Gómez, A., et al. 2011, A&A, 534, A80
Howes, L. M., Asplund, M., Casey, A. R., et al. 2014, MNRAS, 445, 4241
Howes, L. M., Casey, A. R., Asplund, M., et al. 2015, Nature, 527, 484
Johnson, C. I., Rich, R. M., Kobayashi, C., & Fulbright, J. P. 2012, ApJ, 749, 175
Kunder, A., Koch, A., Rich, R. M., et al. 2012, AJ, 143, 57
Lee, Y.-W. 1992, AJ, 104, 1780
Lodders, K., Palme, H., & Gail, H.-P. 2009, Landolt-Börnstein – Group VI Astronomy and Astrophysics Numerical Data and Functional Relationships in Science and Technology Volume 4B: Solar System, ed. J. E. Trümper, 44
Malavolta, L., Piotto, G., Bedin, L. R., et al. 2015, MNRAS, 454, 2621
Martin, W. C., Fuhr, J. R., Kelleher, D. E., et al. 2002, NIST Atomic Database, version 2.0, http://physics.nist.gov/asd, National Institute of Standards and Technology, Gaithersburg, MD
Meléndez, J., & Barbuy, B. 2009, A&A, 497, 611
Meynet, G., Maeder, A., Eggenberger, P., et al. 2016, Astron. Nachr., in press [arXiv:1512.00767]
Minniti, D. 1995, A&A, 303, 468
Modigliani, A., Mulas, G., Porceddu, I., et al. 2004, The Messenger, 118, 8
Montes, F., Beers, T. C., Cowan, J. J., et al. 2007, ApJ, 671, 1685
Ness, M., Freeman, K., Athanassoula, E., et al. 2013, MNRAS, 430, 836
Niu, P., Cui, W., & Zhang, B. 2015, ApJ, 813, 56
Ortolani, S., Bica, E., & Barbuy, B. 1997, MNRAS, 284, 692
Ortolani, S., Barbuy, B., Momany, Y., et al. 2011, ApJ, 737, 31
Phillips, J. G., & Davis, S. P. 1968, The Swan system of the $C_2$ molecule (Univ. of California Press)
Pietrukowicz, P., Udalski, A., Soszuński, I., et al. 2012, ApJ, 750, 169
Pietrukowicz, P., Kozlowski, S., Skowron, J., et al. 2015, ApJ, 811, 113
Piskunov, N., Kupka, F., Ryabchikova, T., et al. 1995, A&AS, 112, 525
Prochaska, J. X., & McWilliam, A. 2000, 537, L57
Renzini, A., D'Antona, F., Cassisi, S., et al. 2015, MNRAS, 454, 4197
Roederer, I. U., Cowan, J. J., Karakas, A. I., et al. 2010, ApJ, 724, 975
Rieke, G. H., & Lebofsky, M. J. 1985, ApJ, 288, 618
Rojas-Arriagada, A., Recio-Blanco, A., Hill, V., et al. 2014, A&A, 569, A103
Rossi, L., Ortolani, S., Barbuy, B., Bica, E., & Bonfanti, A. 2015, MNRAS, 450, 3270
Rossi, L., Ortolani, S., S. Casotto, Barbuy, B., & Bica, E. 2016, MNRAS, submitted
Saha, K., Martinez-Valpuesta, I., & Gerhard, O. 2012, MNRAS, 421, 333
Saito, R. K., Hempel, M., Minniti, D., et al. (VVV Collaboration) 2012, A&A, 537, A21
Siqueira-Mello, C., Chiappini, C., Barbuy, B., et al. 2016, A&A, in press, DOI: 10.1051/0004-6361/201628104
Skrutskie, M., Cutri, R. M., Stiening, & R., et al. 2006, AJ, 131, 1163
Soto, M., Barbá, R., Gunthardt, G., et al. 2013, A&A, 552, A101
Steffen, M., Prakapavicius, D., Caffau, E., et al. 2015, A&A, 583, A57
Stephens, A. W., & Frogel, J. A. 2004, AJ, 127, 925
Travaglio, C., Gallino, R., Arnone, E., et al. 2004, ApJ, 601, 864
Truran, J. W. 1981, A&A, 97, 391
van der Swaelmen, M. 2013, A&A, 560, A44
van der Swaelmen, M., Barbuy, B., Hill, V., et al. 2016, A&A, 586, A1
Walker, A. R., & Terndrup, D. 1991, ApJ, 378, 119
Wanajo, S., & Ishimaru, Y. 2006, Nucl. Phys. A, 777, 676
Yong, D., Alves-Brito, A., Da Costa, G., et al. 2014, MNRAS, 439, 2638
Zoccali, M., Lecureur, A., Hill, V., et al. 2008, A&A, 486, 177

## Appendix A: Equivalent widths and atomic data of Fe I and Fe II lines

**Table A.1.** Fe I and Fe II lines, their wavelengths, excitation potential (eV), oscillator strengths from NIST and VALD3 for Fe I and Fuhr & Wiese (2006) and Meléndez & Barbuy (2009) for Fe II, and equivalent widths (mÅ).

| Species | $\lambda$ (Å) | $\chi_{ex}$ (eV) | log $gf_{NIST}$ | log $gf_{VALD}$ | log $gf_{adopted}$ | 2115 | 2461 | 2939 | 3514 | 5037 | 5485 |
|---|---|---|---|---|---|---|---|---|---|---|---|
| | | | FW06 | MB09 | | | | | | | |
| FeII | 5991.38 | 3.15 | −3.65 | −3.54 | −3.54 | – | 33.8 | – | 24.6 | 27.5 | 26.2 |
| FeII | 6149.25 | 3.89 | −2.84 | −2.69 | −2.69 | 26.3 | 32.9 | 23.5 | 31.4 | 22.3 | 33.0 |
| FeII | 6247.56 | 3.89 | −2.43 | −2.30 | −2.30 | 24.1 | 38.9 | 27.8 | – | 28.0 | 46.1 |
| FeII | 6416.93 | 3.89 | −2.88 | −2.64 | −2.64 | 24.9 | 26.0 | 23.1 | 20.6 | – | 33.5 |
| FeII | 6432.68 | 2.89 | −3.50 | −3.57 | −3.57 | 33.6 | 41.7 | 32.4 | 34.1 | 29.2 | 45.5 |
| FeII | 6516.08 | 2.89 | −3.372 | −3.31 | −3.31 | 45.7 | 59.9 | 47.9 | 51.7 | 44.0 | 64.0 |
| FeI | 5525.544 | 4.231 | – | −1.084 | −1.084 | – | 37.7 | – | – | – | 40.5 |
| FeI | 5543.360 | 4.218 | – | −1.140 | −1.11 | – | 45.5 | – | – | 62.1 | 35.2 |
| FeI | 5554.894 | 4.549 | – | −0.440 | −0.440 | – | 67.9 | 67.8 | – | 74.4 | 48.6 |
| FeI | 5560.211 | 4.435 | – | −1.190 | −1.16 | 39.4 | 29.5 | 41.3 | – | 34.0 | 22.5 |
| FeI | 5567.391 | 2.609 | – | −2.564 | −2.67 | 75.8 | 58.1 | 77.6 | – | 68.0 | 51.2 |
| FeI | 5618.632 | 4.209 | – | −1.276 | −1.276 | 38.3 | 30.5 | 49.5 | – | 34.1 | 34.6 |
| FeI | 5619.595 | 4.387 | – | −1.700 | −1.67 | 31.1 | – | 27.5 | – | 23.6 | – |
| FeI | 5633.946 | 4.991 | – | −0.270 | −0.32 | 44.7 | 44.7 | 56.6 | – | 38.4 | 33.6 |
| FeI | 5638.262 | 4.220 | – | −0.870 | −0.84 | 63.4 | 62.2 | 76.1 | – | 60.6 | 34.9 |
| FeI | 5641.434 | 4.256 | – | −1.180 | −1.15 | 58.8 | 48.3 | 59.5 | – | 60.1 | 39.2 |
| FeI | 5653.865 | 4.387 | – | −1.640 | −1.61 | 26.2 | – | – | – | 20.9 | – |
| FeI | 5679.023 | 4.652 | – | −0.920 | −0.90 | – | 31.8 | 34.5 | – | 42.5 | 36.4 |
| FeI | 5701.544 | 2.559 | – | −2.216 | −2.216 | – | – | – | – | 94.0 | 70.7 |
| FeI | 5706.096 | 4.283 | – | −3.012 | −3.012 | – | 58.3 | – | – | – | – |
| FeI | 5717.833 | 4.284 | – | −1.130 | −1.10 | 28.8 | 28.7 | 36.2 | 46.4 | 42.9 | 37.0 |
| FeI | 6056.005 | 4.733 | – | −0.460 | −0.460 | 48.8 | 42.8 | 54.7 | – | 50.8 | 34.6 |
| FeI | 6078.491 | 4.796 | – | −0.321 | −0.321 | 59.3 | 49.5 | 52.0 | 55.9 | 56.5 | 44.3 |
| FeI | 6079.008 | 4.652 | −1.100 | −1.120 | −1.100 | 30.8 | 31.8 | 26.5 | 24.2 | 31.4 | – |
| FeI | 6082.710 | 2.223 | −3.573 | −3.573 | −3.573 | 67.6 | 48.2 | 61.2 | 50.9 | 53.8 | 24.5 |
| FeI | 6093.643 | 4.608 | −1.470 | −1.599 | −1.470 | 20.8 | – | – | – | 24.2 | – |
| FeI | 6096.664 | 3.984 | −1.880 | −1.930 | −1.88 | 34.4 | 23.8 | 28.9 | 23.1 | 30.5 | – |
| FeI | 6151.617 | 2.176 | −3.299 | −3.299 | −3.299 | 80.9 | 76.2 | 81.1 | 78.2 | 76.2 | 47.5 |
| FeI | 6157.728 | 4.076 | −1.22 | −1.260 | −1.22 | 69.6 | 60.8 | 72.4 | 40.0 | 64.0 | 41.8 |
| FeI | 6165.360 | 4.143 | −1.474 | −1.474 | −1.474 | 53.1 | 44.2 | 47.3 | 49.0 | 49.7 | 42.2 |
| FeI | 6180.203 | 2.728 | −2.649 | −2.586 | −2.649 | 84.4 | 74.9 | 87.3 | 79.7 | 79.0 | 61.7 |
| FeI | 6187.989 | 3.943 | −1.67 | −1.720 | −1.67 | 51.7 | 39.9 | 56.7 | 46.5 | 43.2 | 23.3 |
| FeI | 6200.313 | 2.609 | −2.437 | −2.437 | −2.437 | – | – | – | 97.7 | – | – |
| FeI | 6219.281 | 2.198 | −2.433 | −2.433 | −2.43 | – | – | – | – | – | 97.9 |
| FeI | 6226.734 | 3.884 | – | −2.220 | −2.220 | – | – | 21.6 | – | – | – |
| FeI | 6229.226 | 2.845 | −2.805 | −2.805 | −2.805 | 26.8 | 36.9 | 51.7 | 45.6 | 41.5 | 22.8 |
| FeI | 6240.646 | 2.223 | −3.173 | −3.233 | −3.173 | 75.7 | 54.9 | 74.6 | – | 70.0 | 37.3 |
| FeI | 6246.318 | 3.603 | −0.877 | −0.733 | −0.877 | – | 68.6 | – | – | 90.8 | 80.9 |
| FeI | 6265.132 | 2.176 | −2.550 | −2.550 | −2.550 | – | – | – | – | – | 95.5 |
| FeI | 6270.223 | 2.858 | −2.609 | −2.464 | −2.609 | 76.8 | 64.5 | 68.7 | 60.7 | 66.5 | 44.1 |
| FeI | 6271.278 | 3.332 | −2.703 | −2.703 | −2.703 | 24.8 | 20.8 | 24.9 | – | – | – |
| FeI | 6302.494 | 3.686 | – | −0.973 | −0.973 | 84.7 | 77.9 | 83.7 | – | 85.0 | 62.2 |
| FeI | 6311.500 | 2.832 | −3.141 | −3.141 | −3.141 | 48.8 | 25.9 | 42.8 | 30.4 | 39.0 | – |
| FeI | 6315.306 | 4.143 | −1.232 | −1.232 | −1.232 | 62.8 | 53.5 | 61.0 | 57.3 | 56.0 | 38.9 |
| FeI | 6315.811 | 4.076 | −1.66 | −1.710 | −1.66 | 40.0 | – | 40.0 | 33.0 | 36.8 | 24.4 |
| FeI | 6322.685 | 2.588 | −2.426 | −2.426 | −2.426 | – | 95.1 | – | 95.8 | – | 82.9 |
| FeI | 6336.823 | 3.686 | −0.856 | −0.856 | −0.856 | – | 98.3 | – | – | – | 88.8 |
| FeI | 6344.148 | 2.433 | −2.923 | −2.923 | −2.92 | – | 87.8 | – | 88.8 | 91.0 | 62.1 |
| FeI | 6355.028 | 2.845 | −2.291 | −2.350 | −2.291 | 88.6 | 71.3 | 79.8 | – | 78.3 | 51.7 |
| FeI | 6380.743 | 4.186 | −1.376 | −1.376 | −1.376 | 50.0 | 45.3 | 47.4 | 33.7 | 51.1 | 31.3 |
| FeI | 6392.538 | 2.279 | – | −4.030 | −4.030 | 42.5 | 21.6 | 38.0 | 24.3 | 32.6 | – |
| FeI | 6408.017 | 3.686 | −1.018 | −1.018 | −1.018 | 96.7 | 86.0 | 87.8 | 84.4 | 85.4 | 77.1 |
| FeI | 6411.648 | 3.654 | −0.718 | −0.595 | −0.718 | – | – | – | – | – | 98.9 |
| FeI | 6419.949 | 4.733 | −0.27 | −0.240 | −0.27 | 66.7 | 58.8 | 65.4 | 63.8 | 66.4 | 47.0 |
| FeI | 6469.192 | 4.835 | −0.81 | −0.770 | −0.81 | – | 26.9 | – | – | 38.5 | – |
| FeI | 6475.624 | 2.559 | −2.942 | −2.942 | −2.942 | 76.4 | 64.5 | 81.4 | 68.6 | 83.4 | 50.4 |

**Table A.1.** continued.

| Species | $\lambda$ (Å) | $\chi_{ex}$ (eV) | log $gf_{NIST}$ | log $gf_{VALD}$ | log $gf_{adopted}$ | 2115 | 2461 | 2939 | 3514 | 5037 | 5485 |
|---|---|---|---|---|---|---|---|---|---|---|---|
| FeI | 6481.870 | 2.279 | −2.984 | −2.984 | −2.984 | 96.4 | 79.4 | 98.3 | 89.2 | – | 69.9 |
| FeI | 6498.938 | 0.958 | −4.687 | −4.699 | −4.687 | – | 80.0 | – | 94.8 | – | 58.9 |
| FeI | 6518.366 | 2.832 | −2.298 | −2.460 | −2.298 | 82.0 | 68.5 | 86.8 | – | 76.6 | 53.1 |
| FeI | 6569.214 | 4.733 | −0.450 | −0.420 | −0.450 | 63.4 | 60.5 | 65.2 | 67.2 | 63.1 | 46.2 |
| FeI | 6574.226 | 0.990 | −5.004 | −5.023 | −5.004 | 93.5 | 62.3 | 89.5 | 78.8 | 80.8 | 44.5 |
| FeI | 6575.016 | 2.588 | −2.710 | −2.710 | −2.710 | 95.2 | 79.8 | 93.2 | 85.7 | 83.3 | 65.3 |
| FeI | 6581.209 | 1.485 | −4.679 | −4.679 | −4.679 | 56.8 | 28.3 | 58.4 | 39.7 | 42.2 | 21.7 |
| FeI | 6593.870 | 2.433 | −2.422 | −2.422 | −2.422 | – | – | – | – | – | 92.8 |
| FeI | 6597.559 | 4.796 | −1.050 | −1.070 | −1.05 | 29.5 | 20.6 | 26.4 | 31.7 | 26.3 | – |
| FeI | 6608.025 | 2.279 | – | −4.030 | −4.030 | 39.3 | – | 38.0 | 27.9 | 35.9 | – |
| FeI | 6609.110 | 2.559 | −2.692 | −2.692 | −2.692 | 95.4 | 77.9 | 93.0 | 87.7 | 82.7 | 61.8 |
| FeI | 6627.544 | 4.549 | – | −1.680 | −1.680 | 20.5 | – | – | – | – | – |

## Appendix B: Resulting abundances

In Tables B.1–B.3 are listed line-by-line, the resulting abundance ratios [X/Fe] for the light elements Na, Mg, and Al, the alpha-elements O, Mg, Si, Ca, and Ti, and the heavy elements Eu, Ba, La, Y, Zr, and Sr.

**Table B.1.** Abundances of light elements Na, Mg, Al.

| Species | $\lambda$ (Å) | $\chi_{ex}$ (eV) | log $gf$ | 2115 | 2461 | 2939 | 3514 | 5037 | 5485 | HP1-2 | HP1-3 |
|---|---|---|---|---|---|---|---|---|---|---|---|
| NaI | 5682.633 | 2.102439 | −0.706 | −0.15 | −0.30 | −0.30 | +0.00 | −0.10 | −0.30 | +0.00 | −0.20 |
| NaI | 5688.194 | 2.104571 | −1.400 | +0.20 | −0.30 | −0.15 | -0.20 | −0.10 | −0.30 | −0.10 | −0.20 |
| NaI | 5688.205 | 2.104571 | −0.45 | +0.20 | −0.30 | −0.15 | -0.20 | −0.10 | −0.30 | −0.10 | −0.20 |
| NaI | 6154.230 | 2.102439 | −1.56 | 0.05 | −0.10 | −0.15 | −0.15: | +0.20 | −0.30 | −0.30 | +0.05 |
| NaI | 6160.753 | 2.104571 | −1.26 | +0.25 | −0.15 | −0.15 | +0.10 | +0.30 | +0.00 | −0.30 | – |
| AlI | 6696.185 | 4.021753 | −1.576 | −0.1 | +0.0 | +0.1 | +0.00 | +0.20 | +0.20: | −0.25 | +0.15 |
| AlI | 6696.788 | 4.021919 | −1.421 | – | – | – | – | – | – | – | – |
| AlI | 6698.673 | 3.142933 | −1.647 | −0.10 | +0.10 | 0.00 | +0.10 | +0.20 | +0.20 | −0.30 | +0.20 |
| MgI | 6318.720 | 5.108171 | −2.10 | +0.30 | +0.30 | +0.50 | +0.40 | +0.40 | +0.40 | +0.15 | +0.35 |
| MgI | 6319.242 | 5.108171 | −2.36 | +0.30 | +0.40 | +0.30 | +0.30 | +0.20 | +0.40 | – | +0.30 |

**Table B.2.** Abundance of alpha-elements O, Mg, Si, Ca, Ti.

| Species | $\lambda$ (Å) | $\chi_{ex}$ (eV) | log $gf$ | 2115 | 2461 | 2939 | 3514 | 5037 | 5485 |
|---|---|---|---|---|---|---|---|---|---|
| SiI | 5665.555 | 4.920417 | −2.04 | +0.1 | +0.2 | +0.2 | +0.3 | 0.0 | +0.2 |
| SiI | 5666.690 | 5.616073 | −1.74 | – | – | – | +0.3 | +0.1 | +0.2 |
| SiI | 5690.425 | 4.929980 | −1.87 | +0.3 | +0.2 | +0.3 | +0.3 | +0.2 | +0.0 |
| SiI | 5948.545 | 5.082689 | −1.30 | +0.4 | +0.4 | +0.5 | +0.2 | +0.3 | +0.2 |
| SiI | 6142.494 | 5.619572 | −1.50 | +0.3 | +0.5 | +0.25 | – | +0.2 | +0.1 |
| SiI | 6145.020 | 5.616073 | −1.45 | +0.3 | +0.3 | +0.2 | – | +0.1 | +0.3 |
| SiI | 6155.142 | 5.619572 | −0.85 | +0.2 | +0.2 | +0.4 | +0.4 | +0.2 | – |
| SiI | 6237.328 | 5.613910 | −1.01 | +0.2 | +0.2 | +0.3 | +0.2 | +0.2 | +0.1 |
| SiI | 6243.823 | 5.616073 | −1.30 | +0.2 | – | +0.3 | +0.4 | +0.1 | – |
| SiI | 6414.987 | 5.871240 | −1.13 | +0.3 | +0.4 | +0.4 | +0.3 | +0.4 | +0.2 |
| SiI | 6721.844 | 5.862872 | −1.17 | +0.2 | +0.20 | +0.4 | +0.4 | +0.2 | +0.0 |
| CaI | 5601.277 | 2.525852 | −0.52 | +0.0 | +0.0 | +0.0 | −0.1 | +0.0 | −0.3 |
| CaI | 5867.562 | 2.932710 | −1.55 | +0.1 | +0.1 | +0.0 | +0.3 | +0.0 | – |
| CaI | 6102.723 | 1.879467 | −0.79 | +0.3 | +0.1 | +0.1 | −0.2 | +0.2 | +0.0 |
| CaI | 6122.217 | 1.885935 | −0.20 | +0.0 | +0.1 | +0.0 | +0.0 | +0.2 | +0.1 |
| CaI | 6161.295 | 2.523157 | −1.02 | +0.3 | +0.1 | +0.4 | +0.2 | +0.2 | +0.0 |
| CaI | 6162.167 | 1.899063 | −0.09 | +0.3 | +0.1 | +0.1 | +0.1 | +0.2 | +0.0 |
| CaI | 6166.440 | 2.521433 | −0.90 | +0.3 | +0.0 | +0.4 | +0.1 | +0.3 | +0.0 |
| CaI | 6169.060 | 2.523157 | −0.54 | +0.3 | +0.1 | +0.1 | +0.2 | +0.4 | +0.1 |
| CaI | 6169.564 | 2.525852 | −0.27 | +0.3 | +0.1 | +0.2 | +0.0 | +0.2 | +0.0 |
| CaI | 6439.080 | 2.525852 | +0.30 | +0.3 | +0.0 | +0.1 | +0.0 | +0.4 | +0.1 |
| CaI | 6455.605 | 2.523157 | −1.35 | +0.3 | +0.1 | +0.4 | +0.2 | +0.4 | +0.0 |
| CaI | 6464.679 | 2.525852 | −2.10 | +0.4 | +0.4 | >+0.5 | – | +0.2 | – |
| CaI | 6471.668 | 2.525852 | −0.59 | +0.3 | +0.2 | +0.3 | +0.2 | +0.4 | +0.3 |
| CaI | 6493.788 | 2.521433 | 0.00 | +0.3 | −0.1 | +0.1 | +0.0 | +0.3 | +0.0 |
| CaI | 6499.654 | 2.523157 | −0.85 | +0.3 | +0.0 | +0.3 | +0.1 | +0.2 | +0.0 |
| CaI | 6572.779 | 0.00 | −4.32 | +0.5 | 0.0 | +0.3 | +0.2 | +0.3 | +0.0 |
| CaI | 6717.687 | 2.709192 | −0.61 | +0.4 | +0.2 | +0.5 | +0.3 | +0.5 | +0.1 |
| TiI | 5689.459 | 2.296971 | −0.47 | +0.2 | – | – | +0.1 | – | – |
| TiI | 5866.449 | 1.066626 | −0.84 | +0.1 | +0.0 | +0.2 | +0.0 | +0.3 | – |
| TiI | 5922.108 | 1.046078 | −1.46 | +0.3 | +0.2 | +0.4 | +0.1 | +0.0 | – |
| TiI | 5941.750 | 1.052997 | −1.53 | +0.2 | +0.2 | +0.3 | +0.2 | +0.2 | +0.2 |
| TiI | 5965.825 | 1.879329 | −0.42 | +0.3 | +0.2 | +0.3 | +0.1 | +0.1 | +0.0 |
| TiI | 5978.539 | 1.873295 | −0.53 | +0.3 | +0.1 | +0.2 | +0.2 | +0.2 | +0.0 |
| TiI | 6064.623 | 1.046078 | −1.94 | +0.3 | +0.2 | +0.4 | +0.2 | +0.3 | – |
| TiI | 6091.169 | 2.267521 | −0.42 | +0.3 | +0.2 | +0.3 | +0.3 | +0.0 | +0.3 |
| TiI | 6126.214 | 1.066626 | −1.43 | +0.3 | +0.2 | +0.3 | +0.2 | +0.2 | +0.0 |
| TiI | 6258.110 | 1.443249 | −0.36 | +0.1 | +0.0 | +0.3 | +0.0 | +0.1 | −0.1 |
| TiI | 6261.106 | 1.429852 | −0.48 | +0.3 | +0.1 | +0.2 | +0.0 | +0.0 | −0.1 |
| TiI | 6303.767 | 1.443249 | −1.57 | +0.3 | +0.15 | +0.35 | +0.3 | +0.2 | +0.2 |
| TiI | 6312.240 | 1.460236 | −1.60 | +0.3 | +0.3 | +0.4 | +0.2 | +0.1 | – |
| TiI | 6336.113 | 1.443249 | −1.74 | +0.1 | – | +0.2 | +0.2 | +0.0 | – |
| TiI | 6508.150 | 1.429852 | −2.05 | +0.2 | +0.20 | +0.2 | +0.3 | +0.2 | – |
| TiI | 6554.238 | 1.443249 | −1.22 | +0.1 | +0.0 | +0.2 | +0.2 | +0.1 | −0.15 |
| TiI | 6556.077 | 1.460236 | −1.07 | +0.2 | +0.2 | +0.3 | +0.1 | +0.1 | +0.0 |
| TiI | 6599.113 | 0.899612 | −2.09 | +0.3 | +0.2 | +0.4 | +0.2 | +0.5 | +0.3 |
| TiI | 6743.127 | 0.899612 | −1.73 | +0.3 | +0.1 | +0.3 | +0.3 | +0.1 | +0.2 |
| TiII | 5418.751 | 1.581911 | −2.13 | +0.4 | +0.0 | +0.1 | +0.0 | +0.1 | +0.0 |
| TiII | 6491.580 | 2.061390 | −2.10 | +0.4 | +0.2 | +0.3 | +0.3 | +0.5 | +0.1 |
| TiII | 6559.576 | 2.047844 | −2.35 | +0.4 | +0.3 | +0.3 | +0.2 | +0.5 | +0.3 |
| TiII | 6606.970 | 2.061390 | −2.85 | +0.4 | +0.2 | +0.2 | +0.25 | +0.1 | +0.1 |

**Table B.3.** Abundances of heavy elements.

| Species | $\lambda$ (Å) | $\chi_{ex}$ (eV) | $gf_{adopted}$ | 2115 | 2461 | 2939 | 3514 | 5037 | 5485 | HP1-2 | HP1-3 |
|---|---|---|---|---|---|---|---|---|---|---|---|
| EuII | 6645.064 | 1.379816 | +0.12 | +0.50 | +0.50 | +0.70 | +0.60 | +0.60 | +0.55 | +0.40 | +0.55 |
| BaII | 6141.713 | 0.703636 | −0.076 | +0.50 | +0.30 | +0.50 | −0.10 | +0.70 | +0.50 | +0.50 | +0.50 |
| BaII | 6496.897 | 0.604321 | −0.32 | +0.50 | +0.30 | +0.50 | +0.10 | +0.80 | +0.40 | +0.80 | +0.45 |
| LaII | 6262.287 | 0.403019 | −1.60 | +0.40 | +0.30 | +0.50 | +0.30 | +0.10 | – | – | – |
| LaII | 6320.376 | 0.172903 | −1.56 | +0.30 | +0.00 | +0.30 | +0.25 | +0.00 | – | −0.30 | −0.15 |
| LaII | 6390.477 | 0.321339 | −1.41 | +0.30 | +0.40 | +0.50 | +0.40 | +0.10 | +0.10 | 0.00 | −0.20 |
| YI | 6435.004 | 0.065760 | −0.82 | +0.20 | +0.30 | +0.20 | +0.50 | +0.20: | +0.50 | −0.15 | – |
| YII | 6795.414 | 1.738160 | −1.19 | +0.1 | +0.30 | +0.30 | +0.20 | +0.00 | – | −0.15 | −0.10 |
| ZrI | 6127.475 | 0.153855 | −1.18 | +0.10 | +0.00 | +0.40 | +0.40 | +0.20 | – | – | +0.10 |
| ZrI | 6134.585 | 0.00 | −1.43 | +0.10 | +0.50 | +0.30 | – | +0.20 | – | +0.20: | 0.00 |
| ZrI | 6140.535 | 0.00 | +0.10 | – | +0.50 | – | – | – | (+0.70) | – | |
| ZrI | 6143.252 | 0.070727 | −1.50 | +0.10 | +0.10 | +0.40 | +0.00 | +0.00 | +0.30: | – | −0.15 |
| SrI | 6503.989 | 2.258995 | +0.26 | +0.30 | – | +0.30: | – | +0.30:: | – | +0.50 | +0.30: |
| SrI | 6791.016 | 1.775266 | −0.73 | +0.80: | – | – | – | +0.50:: | – | – | – |